Supplementary Information

Antimicrobial activity, biocompatibility and hydrogelation ability of dipeptide-based amphiphiles

Rajendra Narayan Mitra, Anshupriya Shome, Pritha Paul, and Prasanta Kumar Das*[#]

Department of Biological Chemistry, Indian Association for the Cultivation of Science Jadavpur, Kolkata – 700 032, India.

*To whom correspondence should be addressed. Fax: +(91)-33-24732805, E-mail: bcpkd@iacs.res.in

[#]Also at Centre for Advanced Materials, Indian Association for the Cultivation of Science.

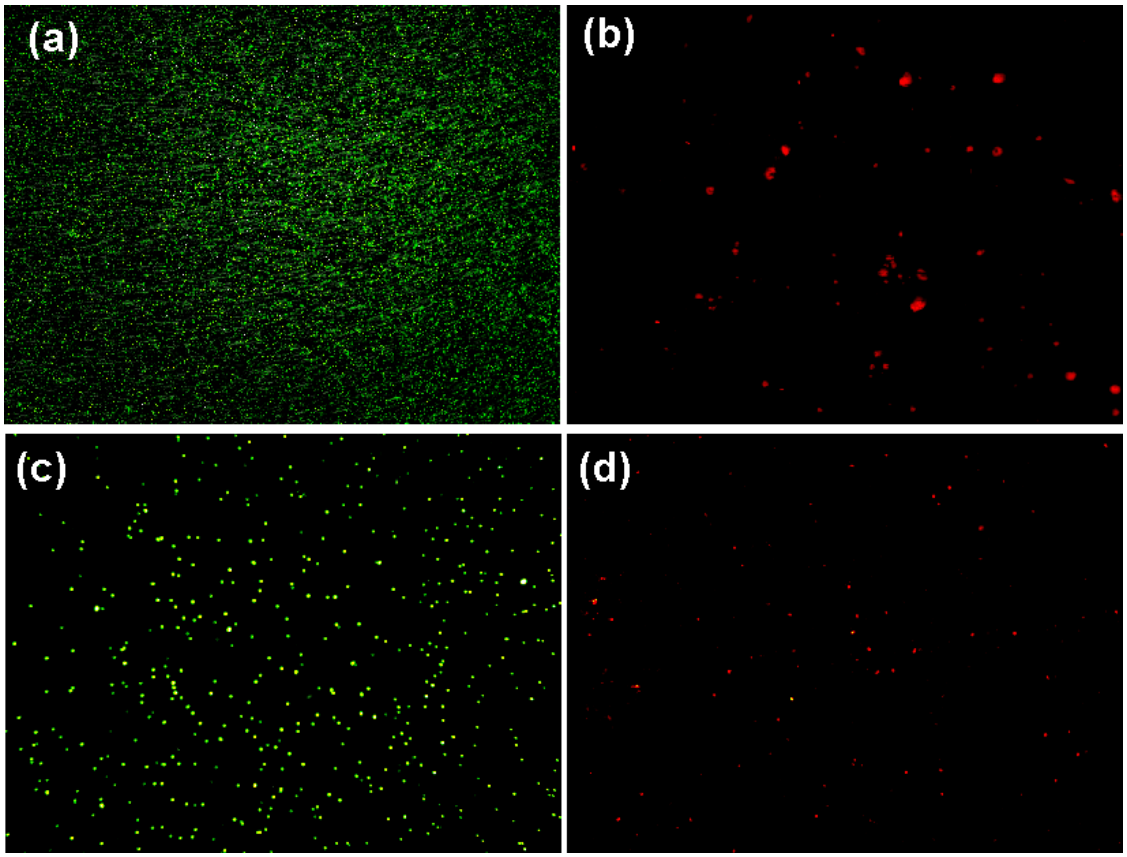

Fig. S1 Fluorescence micrograph of *E. coli* and *S. aureus* before and after treating with compound **1** in presence of LIVE/DEAD® BacLight TM Bacterial Viability Kit; (a) control *E. coli*, (b) *E.coli* treated with 50 µg/mL of **1**, (c) control *S. aureus*, and (d) *S. aureus* treated with 1.0 µg/mL of **1**.

Gelation study of amphiphiles, 1-6

In our earlier study it was observed that the C-16 alkyl chain analogues[1,2] of these dipeptide cationic amphiphiles (Fig. 1, in manuscript) showed hydrogelation ability in plain water at room temperature.[1] In our present study, the C-14 alkyl chain length containing dipeptide amphiphiles (Fig. 1, in manuscript) also exhibit notable hydrogelation efficiencies. The hydrogelation ability was checked by 'stable-to-inversion' of the container method.[1,3-6] Interestingly, minimum gelation concentration (MGC) was found to vary (Table S1) drastically with varying structure of the amphiphiles, **1**-**6**. The observed gelation behaviors of the amphiphiles are in concurrence with their C-16 alkyl chain homologues.[1] The presence of planar aromatic ring in the interior of the polar head (**1** vs. **2**; **3** vs. **4**) improves the hydrogelation efficiency presumably due to the better π-π stacking.[1,4,5] Also the introduction of the extended aromatic ring (in tryptophan) as planar moiety (**1** to **3**; **2** to **4**), improves water gelation ability further (Table S1) with higher thermal stability (Fig. S2). Thus, the presence of the planar aromatic rings both at the interior and exterior region of head group enhances the gelation efficiency for **5** (MGC = 1.8%, w/v) and **6** (MGC = 1.2%, w/v). The amphiphiles showed similar gelation ability in phosphate buffer solution (10 mM, pH = 7.0) as that was observed in plain water. The variations in gel-to-sol transition temperatures (T_{gel}) with concentration of the amphiphiles (Fig. S2) were also in concurrence with previous reports.[1,4-6] The T_{gel} increases from 40 to 52 °C from **1** to **6** because of increase in gelation efficiency driven by strong intermolecular non-covalent interaction. All the hydrogels are thermoreversible in nature as they melt upon slow heating and returned to gel on cooling. The above study indicates the influence of the head group induced supramolecular arrangement of the individual monomer in 3D-network of the hydrogels.

The morphology of supramolecular network of **1**-**6** at MGC was examined by the field emission scanning electron microscopy (FE-SEM, Fig. S3). All dried gels exhibit a typical entangled fibrous network of varying thickness at their MGC. Amphiphiles **1**-**4** showed loosely bound fibrous network of 100-200 nm dimensions while for **5** and **6** that was thin fibrous network with dimension of 50-70 nm. The variation in FE-SEM morphologies of the six dried hydrogels (**1**-**6**) at their MGC values reflects differences in their supramolecular self-assembling pattern in water.

The intrinsic fluorescence probe, tryptophan residue at the polar head group of **5**, was suitably exploited to understand the gelation mechanism/behavior using a concentration (0.0005 to 2%, w/v) dependent and also from a temperature dependent study at the gel state (Fig. S4). The emission intensity at ~355 nm was found to gradually increase with concentration of **5** from 0.0005 to 0.05% w/v, which is ~36 times below to MGC (1.8%, w/v, Table S1). Next, the intensity decreased with further increase in concentration up to 0.25%, w/v (Fig. S4a). Then, the fluorescence intensity attained a steady state at almost 6 times lower concentration (0.3%, w/v) than the MGC indicating the propensity of the amphiphiles to aggregate in the more ordered 3D-dimensional packing. As soon as the self-assembling process initiated towards gelation, probably after 0.05%, w/v, π rings of tryptophan moieties and also ammonium groups are coming close to each other that gradually quenched the fluorescence ability of tryptophan moiety as reflected in its reduced intensity. At the same time, the emission wavelength of tryptophan showed a ~ 35 nm red shift with increase in concentration of **5** from 0.0005%, w/v (355 nm) to 2%, w/v (390 nm). This observed red shift indicates a more polar environment around the tryptophan residue in the gel state. With increase in the concentration of **5**, the quaternary ammonium segment probably fetches more water molecules in its vicinity resulting in a polar environment around the

tryptophan residue. This is consistent with our previous observation where the indole N-H proton of tryptophan showed a continuous upfield shift with increasing amount of water around the gelator.[1,5]

We have also tested the thermoreversibility of hydrogel **5** at the gel state above MGC (4%, w/v) by a temperature dependent luminescence study (Fig. S4b). The fluorescence intensity of tryptophan gradually decreased with unchanged emission wavelength at ~390 nm when the hydrogel was heated from 30 to 80 °C using temperature slope of 5 °C. With the rise in temperature, the non-covalent interactions including hydrophobic interactions, hydrogen bonding, π-π stacking get ruptured and the tryptophan moiety of the amphiphile probably experienced the more hydrophilic environment. At 60 °C and above, the gel phase turned to the solution phase where the intrinsic probe tryptophan is exposed to the water yielding lower fluorescence intensity (Fig. S4b) compared to that at 30 °C. Again in the cooling cycle, the emission intensity increases as the temperature decrease from 80 to 30 °C and remained almost comparable at different temperature. Hence, this experiment indicates the thermoreversible gelation behavior of the amphiphile in water. Interestingly, a break in the slope was observed in the plot of tryptophan emission intensity versus temperature (Fig. S4b). A steady decrease in tryptophan emission intensity was observed from 30 to 60 °C, after which the intensity was still decreasing till 80 °C, but the slope was lower compared to that was observed below 60 °C. Probably at 60 °C, the gel completely converted to solution state because of the destruction of supramolecular non-covalent interactions. And in the solution state the polarity around the tryptophan moiety is no longer changing drastically leading to very low change in its emission intensity. This gel-to-sol transition temperature of **5** at 4%, w/v is in agreement with the T_{gel} value (59 °C) obtained from T_{gel} versus concentration of gelator curve (Fig. S2).

Gelation is fundamentally a transition of a viscous fluid (sol) to an elastic solid state (gel) comprising 3D-supramolecular network structure particularly for low-molecular-weight-gelator (LMWG).[7] The storage modulus (measurement of elastic property) and loss modulus (measurement of fluidity of gel) are commonly described as *G*' and *G*", respectively in rheology. In the sol state, $G''(\omega) > G'(\omega)$ ($G' \sim \omega^2$ and $G'' \sim \omega$; ω= angular frequency) and in gel state $G' > G''$ (G' and $G'' \sim \omega^0$).[8] The crossover point where $G' \approx G''$, provides an accurate measurement of the sol to gel transition from predominantly viscous liquid to elastic solid. Fig. S5a represents the oscillatory viscoelastic temperature ramp curve of hydrogel **5** (4%, w/v) at constant frequency, 1 Hz and 0.2% strain. The storage modulus (*G*') was always greater than the loss modulus (*G*") below the crossover point at 60 °C. At the cross over point, gel melted and the temperature is consistent with the T_{gel} value obtained form the curve in Fig. S3 for **5** at 4%, w/v. Also the tan δ plot with temperature (Fig. S5a) showed a steep rise with temperature above 50 °C being highest at 60 °C, that is equal to the gel melting temperature obtained from the crossover point ($G' \approx G''$). The dynamic viscosity with temperature at a frequency of 1 Hz (Fig. S5b) also showed a broad transition in the vicinity of the gel melting temperature, at 55 °C. Above this temperature, the dynamic viscosity sharply falls due to the destruction of the 3D supramolecular gel network that led to the conversion of gel to solution phase. The rheological data provides the working model of the gel 3D-network, which is expected to have leading information towards its chemical-biology applications.

Experimental

Preparation of hydrogel

The aqueous dispersions of the required amount of compounds (**1**-**6**) were slowly heated to dissolve the compounds in water and then allowed to cool gradually (undisturbed) to room

temperature in a vial with internal diameter (i.d.) of 10 mm. After 20-30 min when the aggregate mass was stable to inversion of the glass vial, the compound was recognized to form a hydrogel.

Determination of gel-to-sol transition temperature (T_{gel})

Gel-to-sol transition temperature (T_{gel}) was determined by placing the hydrogel within an inverted screw-capped glass vial (i.d. of 10 mm) in a thermostatted oil bath and then the temperature was raised at a rate of 2° C/min. Here, the T_{gel} was defined as the temperature (± 0.5° C) at which the hydrogel melts and starts to flow.

Microscopic studies

Field emission scanning electron microscopy (FESEM) measurements were performed on JEOL-6700F microscope. A piece of gel was mounted on a glass slide for SEM sampling, and dried for a few hours under vacuum before imaging. The samples were platinum coated on the surface and were observed at a voltage of 5 kV.

Rheological measurement

Rheological experiments were done using Advanced Rheometer AR 2000 (TA Instruments, USA). All the rheological experiments were done by cone and plate geometry (diameter was 40 mm) on the peltier plate. The hydrogel **5** was prepared as mentioned above and was transferred on the peltier plate to remove the air gap with cone. The temperature sweep experiment was done from 10 to 70 °C at the heating rate of 5 °C/min using frequency 1 Hz, and strain 0.2%.

Table S1 Gelation results of **1-6** in plain water at room temperature

Amphiphiles	State[a]	MGC (%, w/v)	T_{gel} (°C) at MGC
1	OG	22	40
2	TG	18	42
3	OG	13	48
4	TG	10	54
5	TG	1.8	50
6	TG	1.2	52

[a] TG: transparent hydrogel, OG: opaque hydrogel.

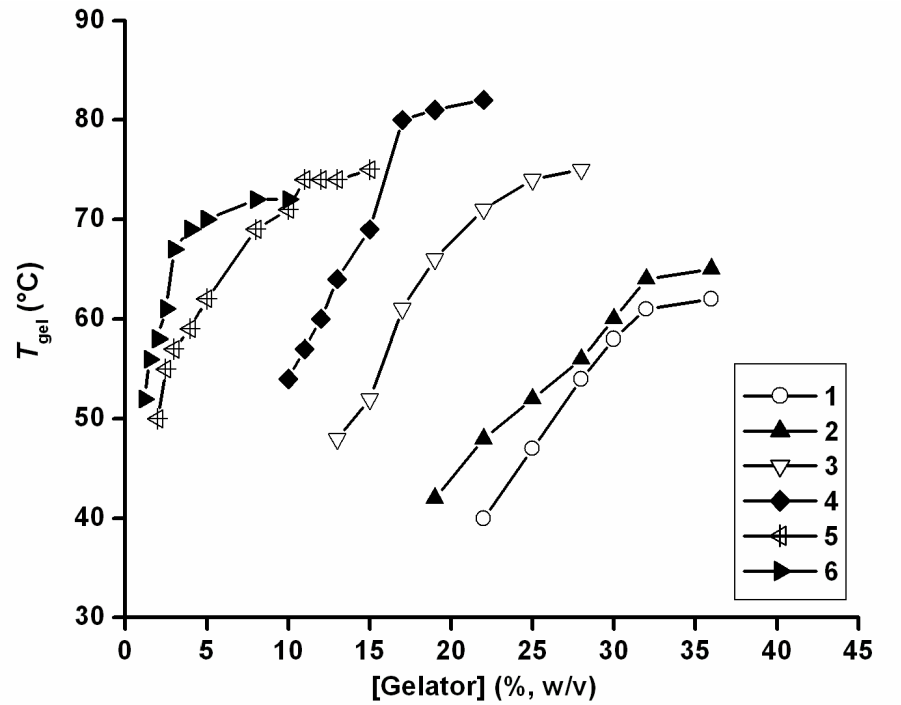

Fig. S2 Variation of the gel-to-sol transition temperature (T_{gel}) with the gelator concentrations.

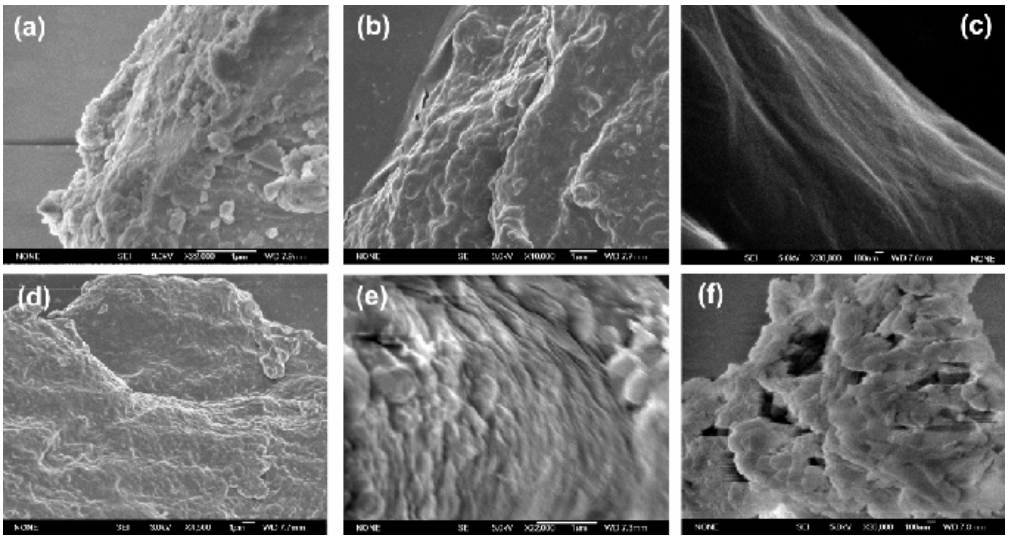

Fig. S3 FE-SEM images of the dried gels of **1-6** (a-f), respectively at the corresponding MGCs.

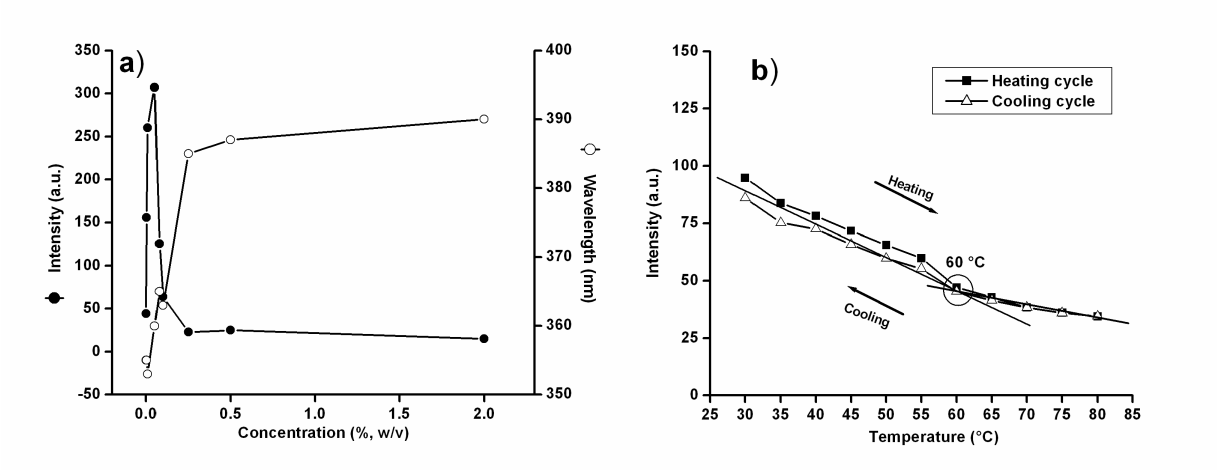

Fig. S4 (a) Variation of tryptophan fluorescence emission intensity and wavelength with concentration of **5** from 0.0005 to 2%, w/v; (b) Variation of tryptophan fluorescence emission intensity (at 390 nm) with heating and cooling cycles from 30-80 °C of hydrogel **5** at 4%, w/v. The excitation wavelength = 285 nm.

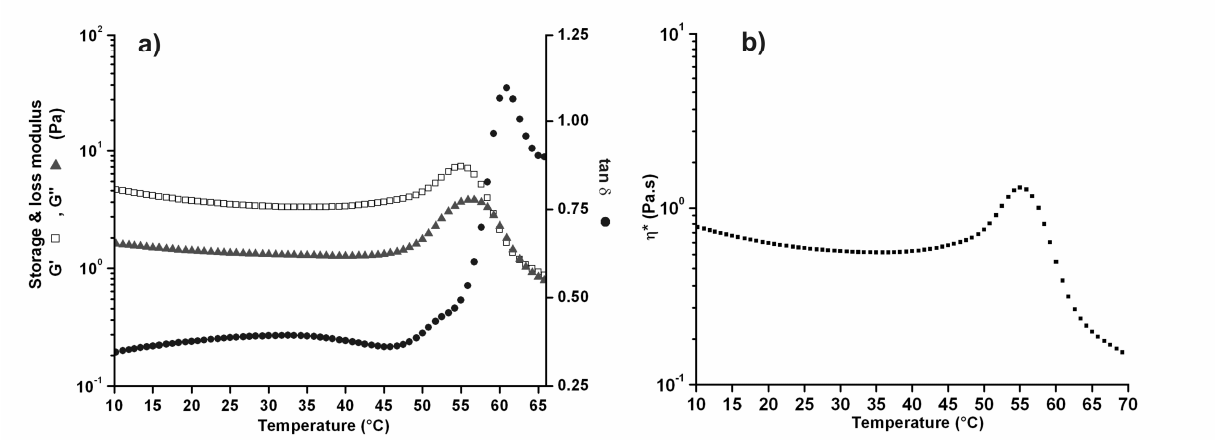

Fig. S5 (a) The oscillatory viscoelastic temperature ramp curve of gel **5** (4%, w/v) at a constant frequency 1Hz and 0.2% strain. (b) The oscillatory temperature ramp curve of dynamic viscosity versus temperature of the gel **5** (4%, w/v) at a constant frequency 1Hz and 0.2% strain.

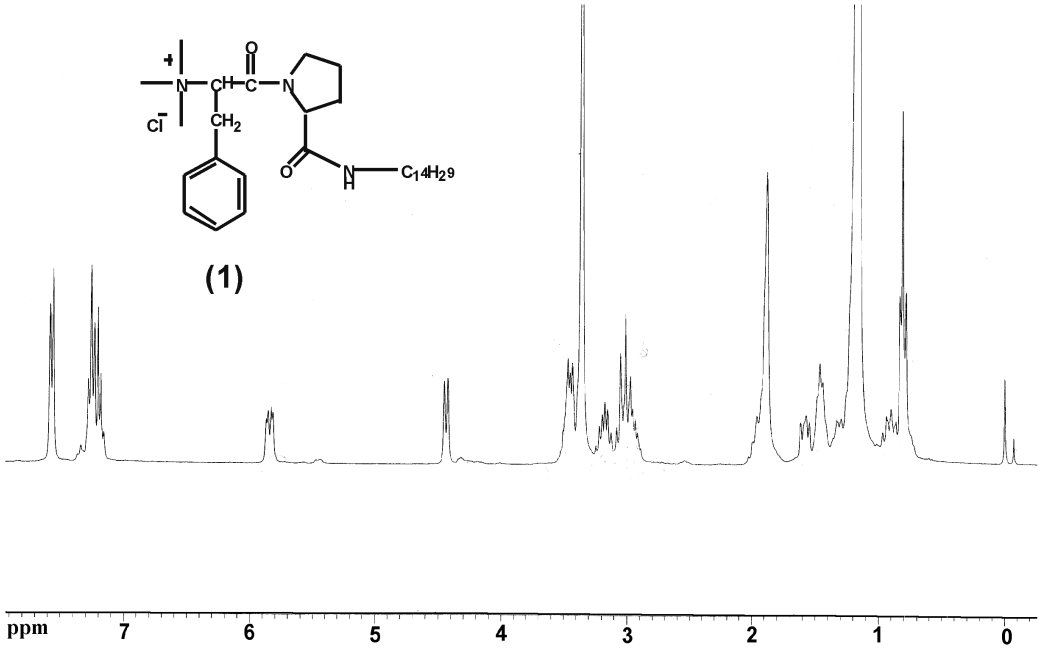

Fig. S6 300 MHz ^{1}H NMR spectra of amphiphile **1** in $CDCl_3$.

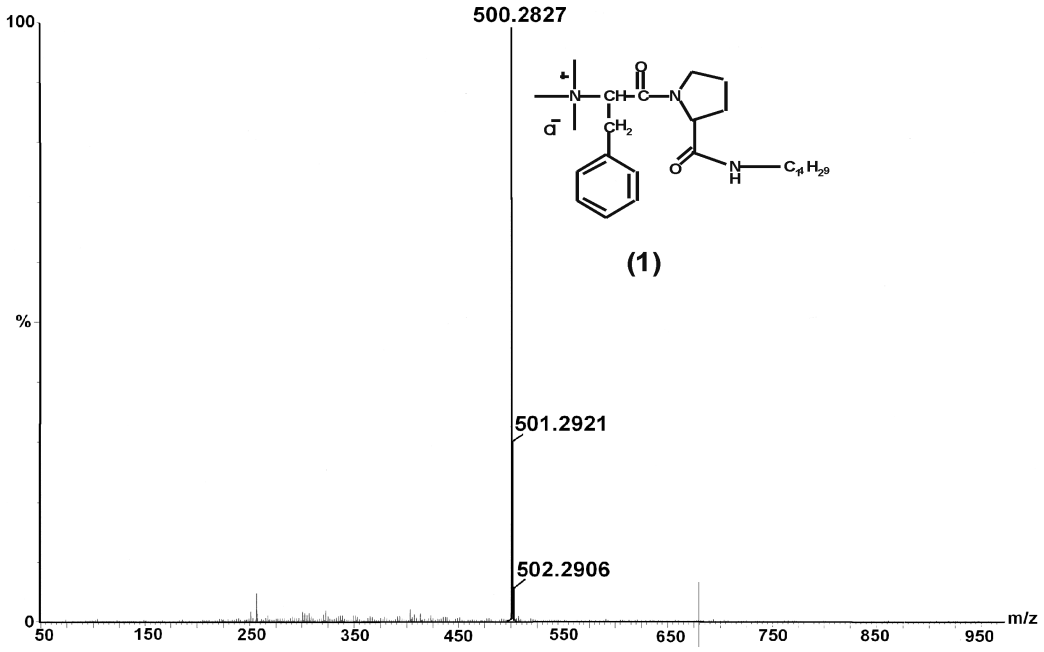

Fig. S7 ESIMS spectra of amphiphile **1**.

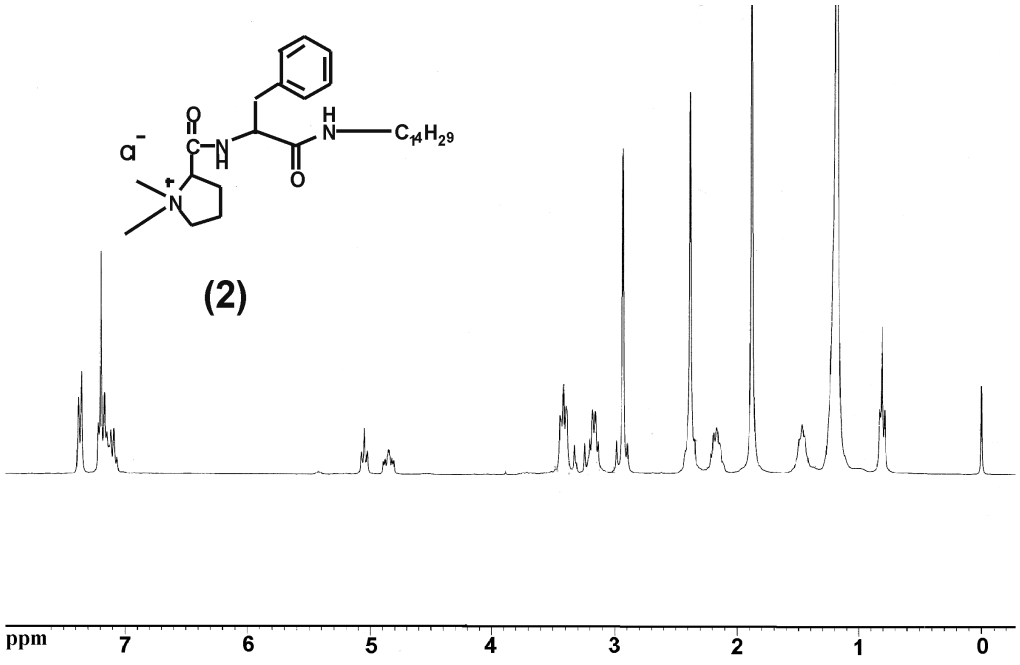

Fig. S8 300 MHz ^{1}H NMR spectra of amphiphile **2** in $CDCl_3$.

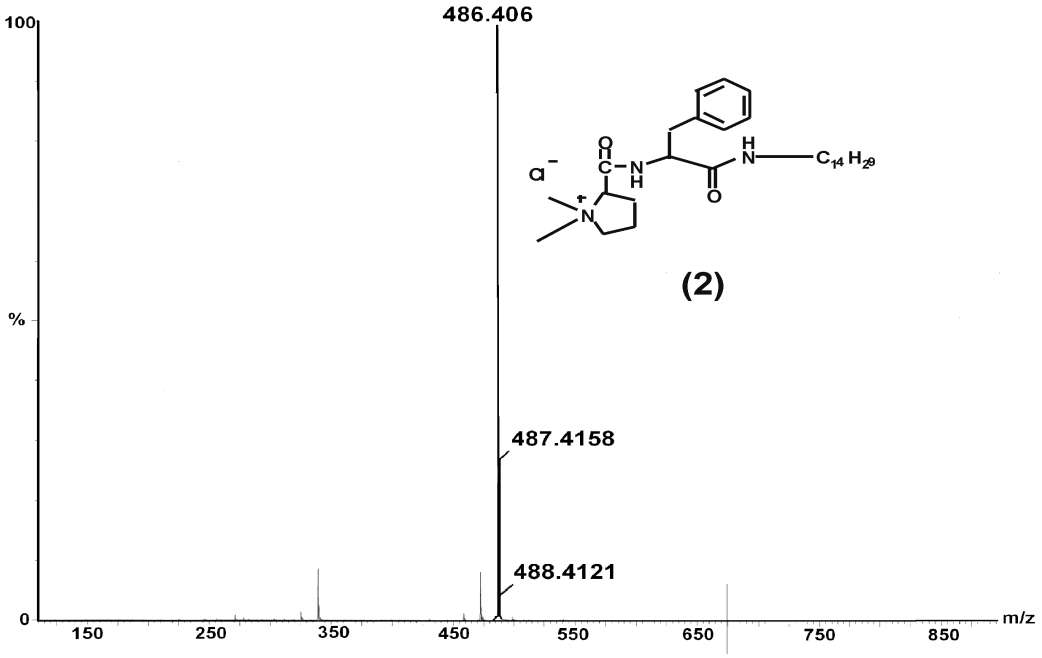

Fig. S9 ESIMS spectra of amphiphile **2**.

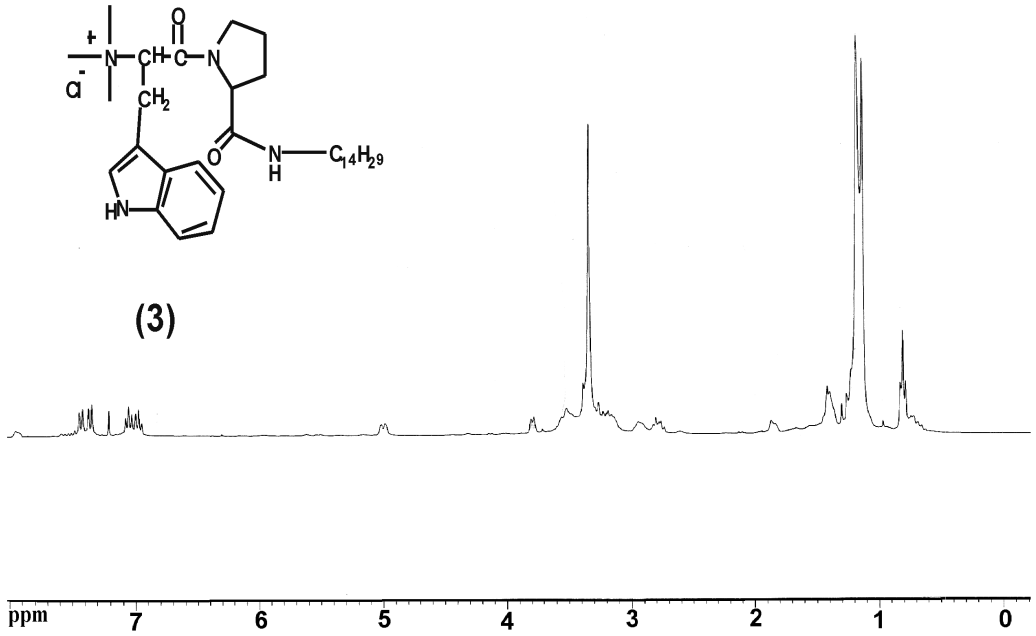

Fig. S10 300 MHz ^{1}H NMR spectra of amphiphile **3** in $CDCl_3$.

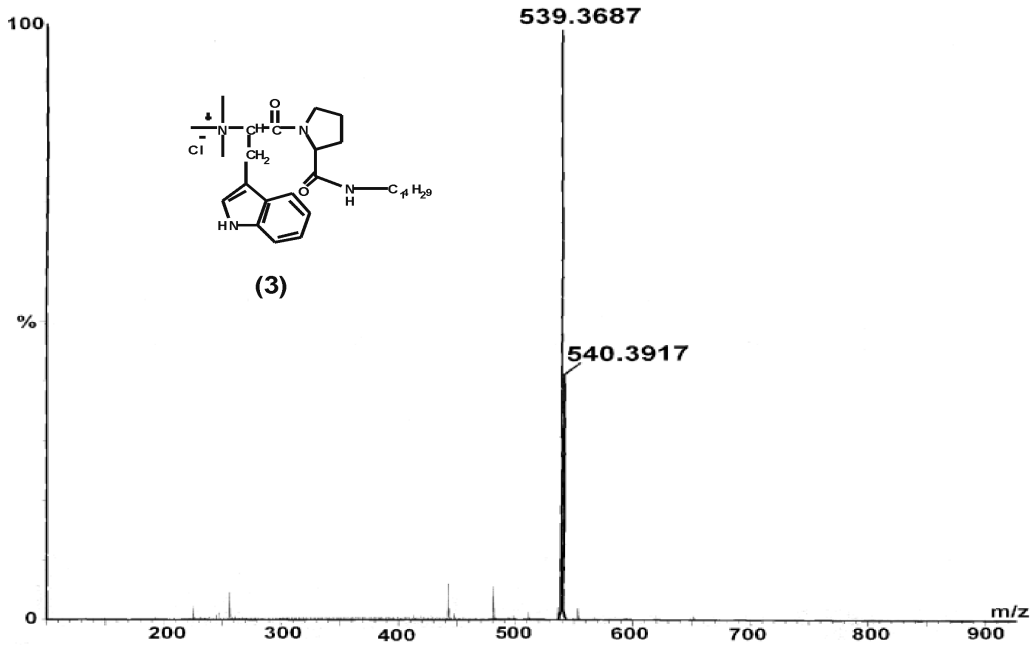

Fig. S11 ESIMS spectra of amphiphile **3**.

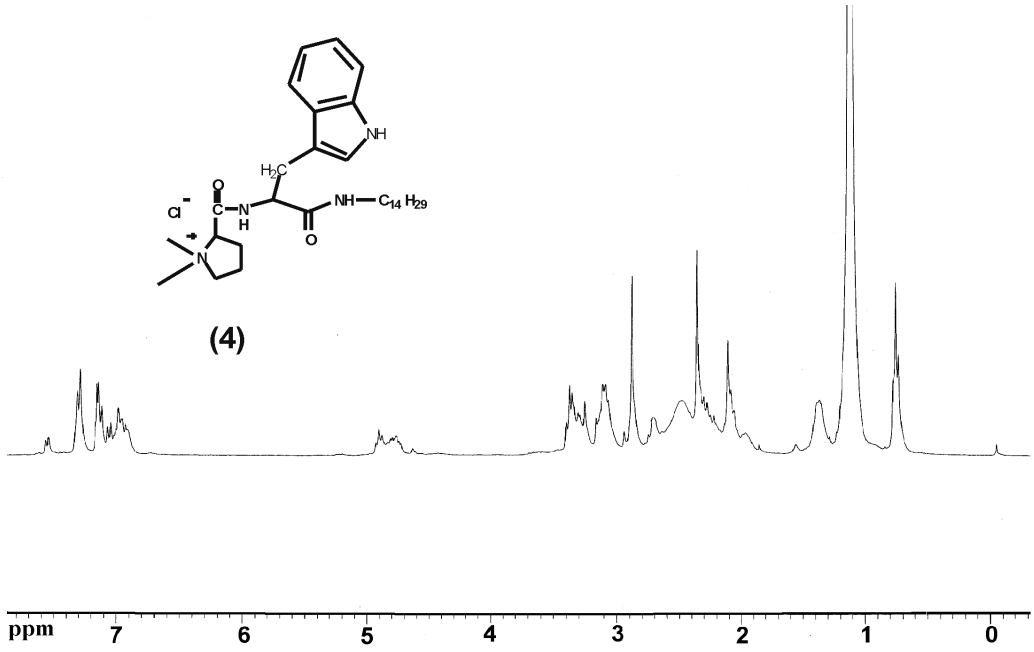

Fig. S12 300 MHz ^{1}H NMR spectra of amphiphile **4** in $CDCl_3$.

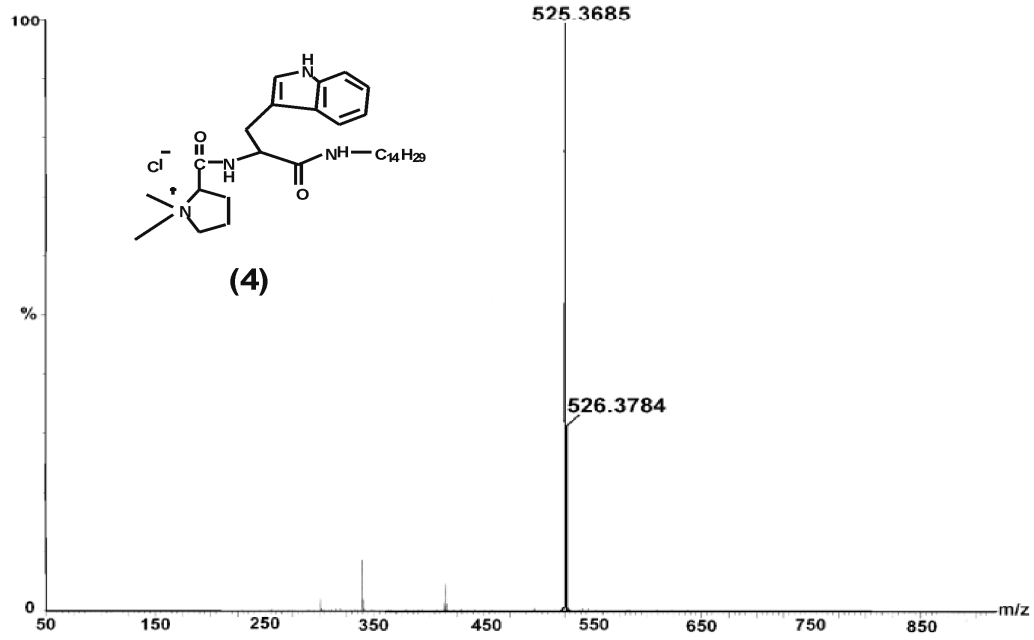

Fig. S13 ESIMS spectra of amphiphile **4**.

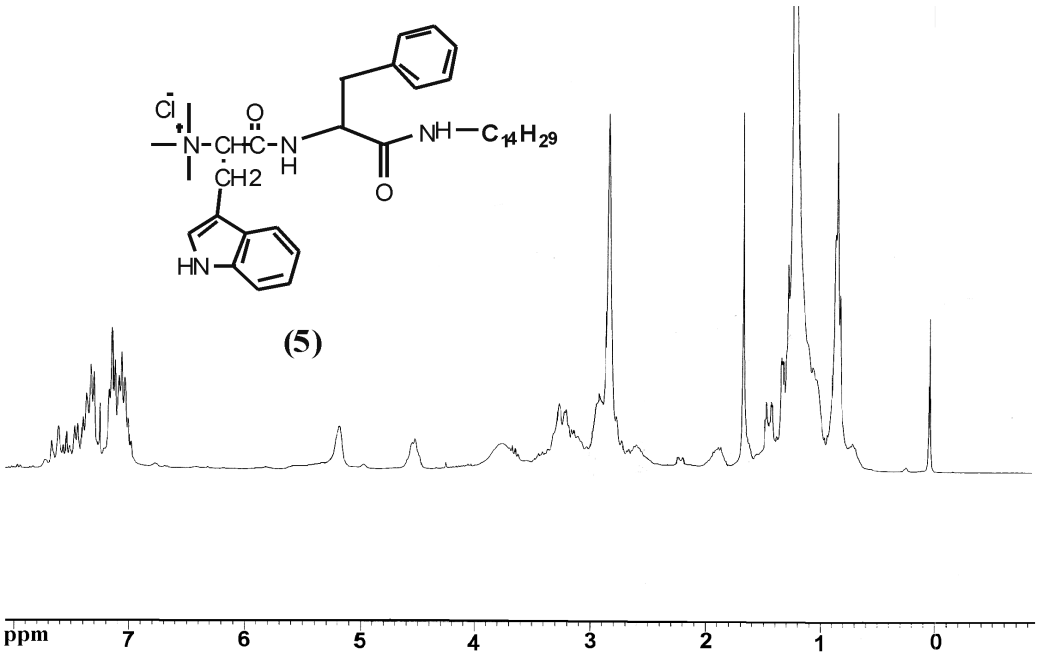

Fig. S14 300 MHz ^{1}H NMR spectra of amphiphile **5** in $CDCl_3$.

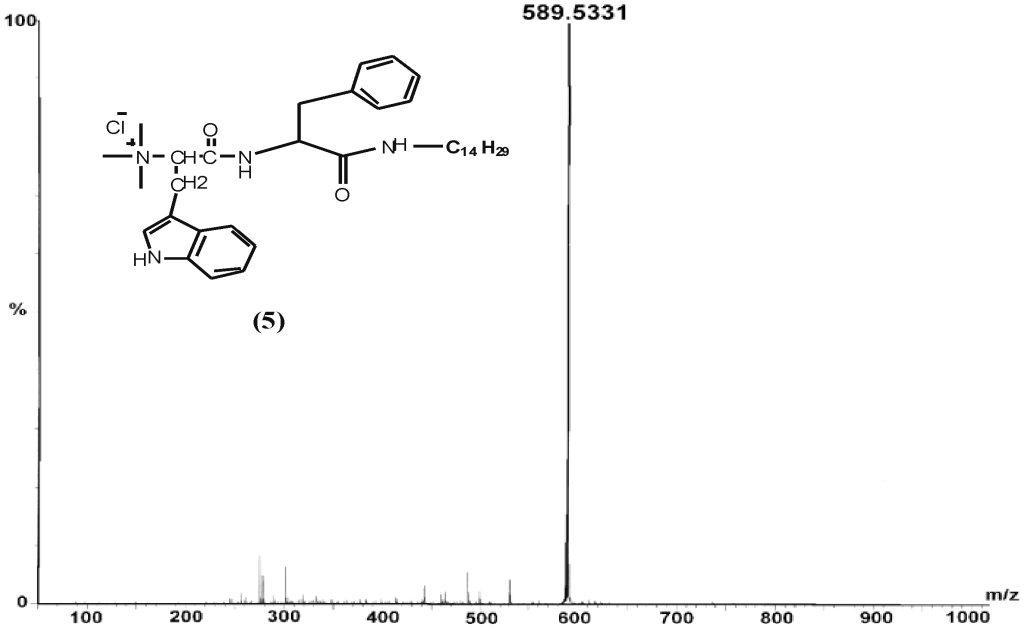

Fig. S15 ESIMS spectra of amphiphile **5**.

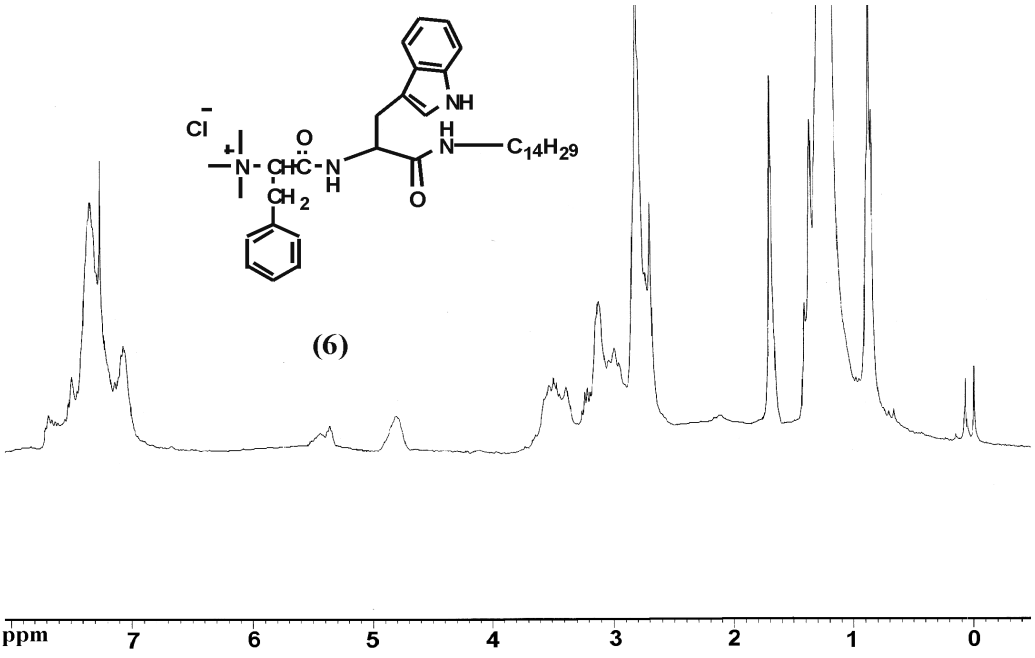

Fig. S16 300 MHz ^{1}H NMR spectra of amphiphile **6** in $CDCl_3$.

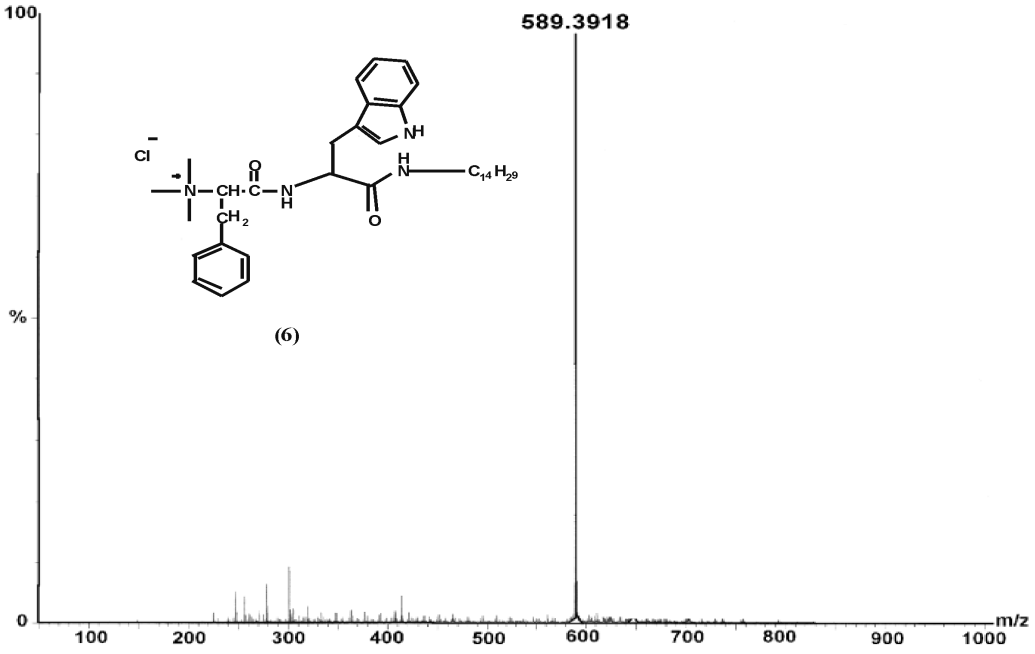

Fig. S15 ESIMS spectra of amphiphile **6**.

Reference

1 R. N. Mitra, D. Das, S. Roy and P. K. Das, *J. Phys. Chem.* B, 2007, **111**, 14107-14113.

2 A. Dasgupta, R. N. Mitra, S. Roy and P. K. Das, *Chem. Asian J*., 2006, **1**, 780-788.

3 A. Takahasi, M. Sakai and T. Kato, *Polymer Journal*, 1980, **12**, 335-341.

4 D. Das, A. Dasgupta, S. Roy, R. N. Mitra, S. Debnath and P. K. Das, *Chem. Eur. J*., 2006, **12**, 5068-5074.

5 S. Roy, A. Dasgupta and P. K. Das, *Langmuir*, 2007, **23**, 11769-11776.

6 A. Shome, S. Debnath and P. K. Das, *Langmuir*, 2008, **24**, 4280-4288.

7 A. M. Smith, R. J. Williams, C. Tang, P. Coppo, R. F. Collins, M. L. Turner, A. Saiani and R. V. Ulijn, *Adv. Mater*., 2008, **20**, 37–41; A. M. Bieser and J. C. Tiller, *J. Phys. Chem. B*, 2007, **111**, 13180-13187.

8 M. Tiitu, P. Hiekkataipale, J. Hartikainen, T. Makela and O. Ikkala, *Macromolecules*, 2002, **35**, 5212-5217.